Journal of Nanophotonics

Nanophotonics.SPIEDigitalLibrary.org

Differential cross section for reflected electrons measured by electron mirror method

Younis Mohamed Atiah Al-zahy

SPIE.

Differential cross section for reflected electrons measured by electron mirror method

Younis Mohamed Atiah Al-zahy*
Misan University, College of Dentistry, Al Amarah 62001, Iraq

Abstract. We derive an equation for the differential cross-section $d\sigma/d\Omega$ of reflected electrons by using Electron Mirror method. The mathematical derivation of differential cross-section equation is based on the Rutherford scattering model as well as the equation of electric potential difference. We describe the interaction of focused electron beams with a polyethylene terephthalate sample using focused ion beam-scanning electron microscope electron mirror image. The electron differential cross-section $d\sigma/d\Omega$ for different working distances $h = 33$, 20, and 10 mm, with a scattering angle θ ranged from 10 deg to 55 deg, incident electrons energies $\eta = 500$, 750, and 1000 eV, and scanning potential $\Delta\varphi$ ranged from 1 to 2 kV has been calculated. According to our findings, the differential cross-section $d\sigma/d\Omega$ of reflected electrons decreases with increasing scattering angle θ and the working distance h and is directly proportional to the difference potential $\Delta\varphi$ and the energy of incident electrons η. Distort the electron mirror images with increased $\Delta\varphi$. © *2015 Society of Photo-Optical Instrumentation Engineers (SPIE)* [DOI: 10.1117/1.JNP.9.093096]

Keywords: scanning electron microscope; electron mirror effect; electron diffraction; insulator; secondary electrons; charging.

Paper 14104 received Oct. 7, 2014; accepted for publication Dec. 17, 2014; published online Jan. 23, 2015.

1 Introduction

A scanning electron microscope is an instrument for observing and analyzing the microscopic characteristics of a wide variety of samples using a focused beam of high energy electrons. When nonconductive samples, such as PVC,[1] a-SiO_2,[2] polyester,[3] and a polyethylene terephthalate (PET) irradiated by electron radiation with sufficiently high energy, the scanning electron microscope analysis fails.[3]

The charging effects in an electron irradiated insulators results from a competition between the secondary electron (SE) emission which contributes to a positive charging, and the trapping of electrons by the sample. Due to the localization of the injected electrons and secondary emission as well as defects produced during electron irradiation, the sign of the trapped charge and the resulting macroscopic surface potential may locally change between positive and negative.[4–6]

When charged particles impinge on a solid they can impart energy, exciting electrons within the material. If this energy is sufficient to overcome surface energy barriers (e.g., work function or electron affinity) electrons can escape from the material, leading to material charging. The emitted electrons can be divided into two categories: (a) SEs; typically lower energy electrons (<50 eV by convention) that originate within the material, produced by numerous inelastic scattering events of the incident electrons; (b) backscattered electrons; typically higher energy electrons (>50 eV by convention) that originate from the incident electron source, but scatter either elastically or inelastically before leaving the target material.[7–9]

Usually, the interaction of the electron beam with an insulator results in patterns of the electric field of the trapped charges. The electrons are repelled by the negative charge on the sample and sent in another direction where they interact normally with another sample (inner chamber

*Address all correspondence to: Younis Mohamed Atiah Al-zahy; E-mail: younisal_zahy72@yahoo.co.uk

materials) that generates SEs, some of which are collected by the sensor. Via this mechanism, the sample itself becomes a mirror.[10]

The pseudomirror effect is a phenomenon that was first described by Belhaj et al.,[11] in which both the reflected electrons and the SEs generated on the sample surface could be detected.

Belhaj et al.[12] studied the influence of the primary beam energy on the sign and the amount of trapped charge and also illustrated the ability of the method to study the kinetics of the electron trapping-detrapping phenomena.

In 1999, Vallayer et al.[13] published a paper in which they described a method to determine the number of charges that are trapped on the surface of an insulator and which led to important information about the mirror effect phenomena and the insulator properties.

By 2001, Croccolo and Riccardi observed a mirror image using an ion beam, where the sample is positively charged by the ion beam impinging on a nonconducting sample. This effect appears to be the sum of the ion implantation/neutralization plus the electron emission and is supposed to have exponential dynamics. Eventually, the sample is observed with lower energy ions. If the energy is sufficiently small relative to the deposited charge, ions are reflected back by the Coulomb repulsion and hit the focused ion beam (FIB)/scanning electron microscope (SEM) chamber. The interaction of the chamber material with the ions gives rise to electron emission and some of these electrons are detected by the active detector giving rise to a mirror image.[1]

Additionally, Wintle[14] and Liebault et al.[15] used the mirror image method as a tool to determine the charge trapped in dielectric samples. The study of Milani et al.[16] shows the importance of the possible paths of electrons traveling in the chamber of an electron microscope when an electrostatic field is present on the specimen surface. However, much of the research up until now has been descriptive in nature of the electron mirror image such as that of Al-zahy et al.[17] and Hattali et al.[18]

This project provided an important opportunity to advance the understanding of the potential distribution on a charged disc-area generated when a scanning electron microscope is used as a source of electrons. The major objective of this study was to investigate the differential cross-section $d\sigma/d\Omega$ of reflected electrons from a charged disc-area for different scattering angles θ, scanning potentials $\Delta\varphi$, working distances h, and electron energy η.

The present manuscript is organized in four sections, including the introductory one. Section 2 deals with a description of a scanning electron microscope with an FIB and PET sample. Section 3 summarizes the theoretical background of the research and eventually derives an equation for the differential cross-section $d\sigma/d\Omega$ of reflected electrons according to the Rutherford scattering model and the distribution of the electric field at the surface of the charged disc area. Section 3 also focuses on three main aspects: In Sec. 3.1, we focus on the surface potential of the sample versus the radius of the charged disc area and the working distance (h). In Sec. 3.2, we derive an equation for the trapped charge Q as a function of the working distance (h) and the potential difference ($\Delta\varphi$) and use it to discuss how the trapped charge Q of the (PET) sample is affected both by varying (h) and ($\Delta\varphi$) inside the FIB-SEM system. In Sec. 3.3, we deal with the differential cross-section $d\sigma/d\Omega$ of reflected electrons versus the working distance h, energy of incident electrons η, scattering angle θ, and the potential difference $\Delta\varphi$. Finally, the conclusion gives a brief summary and critique of the findings.

2 Material and Methods

A scanning electron microscope (SEM) with an FIB (FEI, Quanta 3D) is a powerful magnification tool that utilizes focused beams of electrons or ions to obtain information. Three-dimensional images produced by SEMs provide topographical, morphological, and compositional information, which makes it invaluable in a variety of science and industry applications. The FIB is a tool that basically performs three functions: ion imaging (from SEs or ions), milling (precision down to 10 nm), and deposition (with the insertion of a small needle delivering special precursor gases). The FIB-SEM system has been used to generate the electron mirror image by using PET as sample as shown in Fig. 1. The samples are ~99% pure PET in the form of cylinders, 1.5-mm thick and 4 mm in diameter. The practical part (electron mirror images) of the research was conducted at the Department of Material Sciences of the University of Milano-Bicocca, FIB-SEM Bombay Lab Via Cozzi 53, I–20125 Milano.

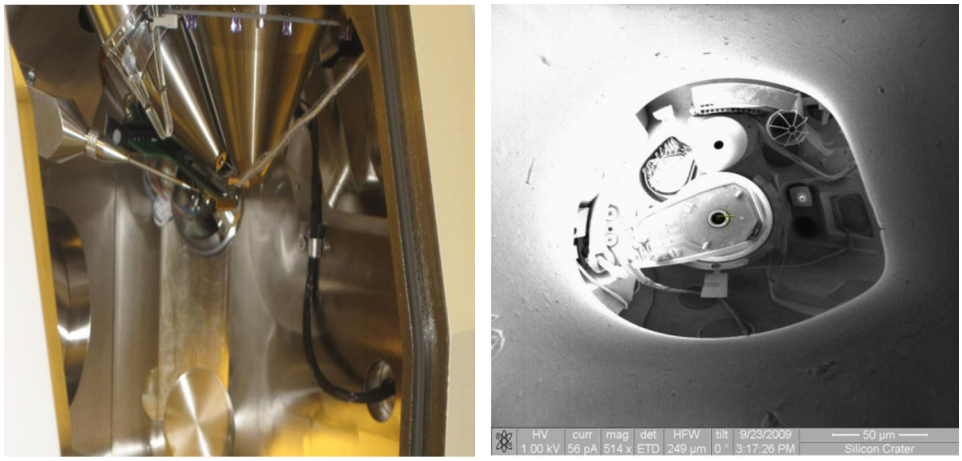

Fig. 1 Electron mirror effect image from the polyethylene terephthalate (PET) sample versus photograph of the top focused ion beam/scanning electron microscope system.

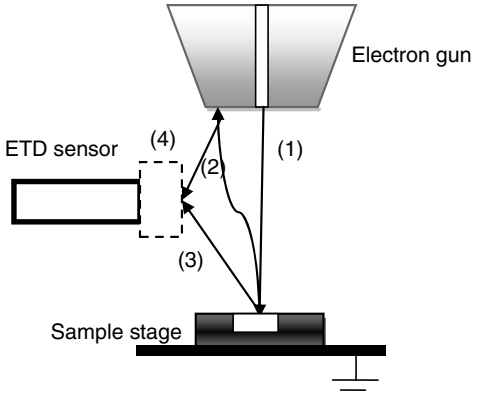

Fig. 2 Schematic of electron mirror image.

3 Results and Discussion

3.1 *Measurement of Surface Potential*

Figure 2 shows the working principle when the insulator sample is irradiated with electrons that are reflected back from the charged PET sample. Arrow (1) indicates the incident electrons of the electron gun scanning the surface of PET sample. The wavy arrow (2) indicates electrons reflected back from the charged PET sample and interaction with materials of the top wall of FIB-SEM chamber. Arrow (3) refers to electrons reflected back from the charged PET sample and these electrons are detected by an Everhard-Tornley detector (ETD). Arrow (4) shows the SEs generated from the interaction of electrons with the top wall of the FIB-SEM chamber; these SEs are detected by ETD giving rise to the mirror image. The scanned area accumulates charge and its surface potential increases.[19]

When the scanning electron microscope is used as a source of energetic electrons, the disc-charged area is produced. A disc of radius R is uniformly charged with a total charge Q. This study first evaluates the magnitude of the electric field at point O lying a distance h from the center of the disc along the axis of symmetry of the disc as shown in Fig. 3.

The electric field at point O due to a group of point charges $\mathrm{d}q$ can be obtained as[20]

$$\mathrm{d}E = \frac{k}{(\varepsilon_r + 1)} \frac{\mathrm{d}q}{y^3} h, \tag{1}$$

where k is the Coulomb constant, $y = \sqrt{(h^2 + r^2)}$, ε_r is the permittivity of the PET sample, $\mathrm{d}q$ is a differential element of the charge distribution, h is the working distance (i.e., distance between

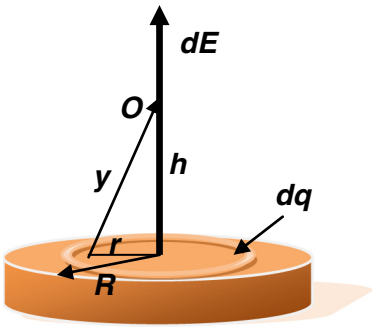

Fig. 3 Schematic illustration of the electric field of a disc charged area.

the electron gun aperture and the insulator surface), r is the distance from the center of the disc to dq, and dE is the electric field established at that point. If the charge distribution is continuous rather than being a collection of points, Eq. (1) must be replaced by an integral

$$E = \int \mathrm{d}E = \frac{k}{(\varepsilon_r + 1)} \int \frac{\mathrm{d}q}{\sqrt{(h^2 + r^2)^3}} h. \tag{2}$$

Set up the basic equations

$$\mathrm{d}q = \delta \mathrm{d}A = 2\pi r \delta \mathrm{d}r, \tag{3}$$

where δ is a surface charge density and dA is a differential element of the charged disc area. We substitute Eq. (3) into Eq. (2), and obtain the equation

$$E = \frac{\pi \delta k h}{(\varepsilon_r + 1)} \int_0^R \frac{2r\mathrm{d}r}{\sqrt{(h^2 + r^2)^3}}. \tag{4}$$

By solving the integral in Eq. (4), we obtain

$$E = \frac{\pi k h \delta}{(\varepsilon_r + 1)} \left(\frac{1}{h} - \frac{1}{\sqrt{(h^2 + R^2)}} \right), \tag{5}$$

where

$$Q = \pi R^2 \delta. \tag{6}$$

Insertion of Eq. (6) into Eq. (5) yields the electric field of the total charge:

$$E = \frac{Qk}{(\varepsilon_r + 1)R^2} \left(1 - \frac{h}{\sqrt{(h^2 + R^2)}} \right). \tag{7}$$

By using an incident electron which was normal to the PET sample, the sample was charged and such a charge resulted in a potential distribution, the potential of the charged disc can be found by

$$\varphi = -\int E \mathrm{d}h. \tag{8}$$

We substitute Eq. (7) into Eq. (8), and obtain the equation

$$\varphi\,(R,\ h) = \frac{Qk}{R^2(\varepsilon_r + 1)} [\sqrt{(h^2 + R^2)} - h]. \tag{9}$$

Equation (9) provides a shortcut to understanding the behavior of the potential φ (R, h), which depends on the working distance h and the radius of the charged disc R.

Suppose we would like to find the potential φ (R, h) of the electron gun by rewriting Eq. (9) in the following form:

$$\varphi(R,h) = \frac{Qkh}{R^2(\varepsilon_r+1)}\left\{\left[1+\left(\frac{R}{h}\right)^2\right]^{\frac{1}{2}}-1\right\}. \tag{10}$$

To simplify Eq. (10), use the series expansion of the square root as follows:

$$\left[1+\left(\frac{R}{h}\right)^2\right]^{\frac{1}{2}} = 1+\frac{1}{2}\left(\frac{R}{h}\right)^2-\frac{1}{8}\left(\frac{R}{h}\right)^4+\frac{1}{16}\left(\frac{R}{h}\right)^6-\frac{15}{128}\left(\frac{R}{h}\right)^8+\ldots. \tag{11}$$

At $h \gg R$, the following approximation is helpful

$$\left[1+\left(\frac{R}{h}\right)^2\right]^{\frac{1}{2}} \cong 1+\frac{1}{2}\left(\frac{R}{h}\right)^2. \tag{12}$$

This approximation can be substituted into Eq. (10) to yield

$$\varphi(R,h) \cong \frac{Qkh}{R^2(\varepsilon_r+1)}\left\{\left[1+\frac{1}{2}\left(\frac{R}{h}\right)^2\right]-1\right\}, \qquad h>0. \tag{13}$$

The potential at the surface of the electron gun is

$$\varphi(R,h)_{\text{gun}} \cong \frac{Qk}{h(\varepsilon_r+1)}. \tag{14}$$

Equation (9) can be used to find the potential above the surface of sample; we rearrange Eq. (9) to give

$$\varphi(R,h) = \frac{Qk}{R^2(\varepsilon_r+1)}\left\{R\sqrt{\left[\left(\frac{h}{R}\right)^2+1\right]}-h\right\}, \qquad h>0. \tag{15}$$

The following binomial series is helpful:

$$\left[1+\left(\frac{h}{R}\right)^2\right]^{\frac{1}{2}} = 1+\frac{1}{2}\left(\frac{h}{R}\right)^2-\frac{1}{8}\left(\frac{h}{R}\right)^4+\frac{1}{16}\left(\frac{h}{R}\right)^6-\frac{15}{128}\left(\frac{h}{R}\right)^8+\ldots. \tag{16}$$

For this situation $R \gg h$, Eq. (16) can be expressed as

$$\left[1+\left(\frac{h}{R}\right)^2\right]^{\frac{1}{2}} \cong 1+\frac{1}{2}\left(\frac{h}{R}\right)^2. \tag{17}$$

We substitute Eq. (17) in Eq. (15) to yield

$$\varphi(R,h) \cong \frac{Qk}{R^2(\varepsilon_r+1)}\left\{R\left[1+\frac{1}{2}\left(\frac{h}{R}\right)^2\right]-h\right\}, \tag{18}$$

when the incident electron beam is close to the sample surface $R \gg h$, $h \cong 0$, $1/2(h/R)^2 \cong 0$, therefore, Eq. (18) becomes

$$\varphi(R,h)_{\text{sample}} \cong \frac{Qk}{R(\varepsilon_r+1)}\left(1-\frac{h}{R}\right). \tag{19}$$

At $R \cong 0$, $h = 0$, the value $(1 - h/R) = 1$, and the potential at the center of the disc is given by

$$\varphi(R,h)_{\text{disc center}} \cong \frac{Qk}{R(\varepsilon_r + 1)}. \tag{20}$$

The magnitude of the potential increases and reaches its maximum value at $R \cong 0$.

The "fast" electrons travel through a working distance h and begin decelerating to low energies near the sample surface. The potential difference between the electron gun and the sample surface is

$$\Delta\varphi(R,h) = \varphi_{\text{gun}} - \varphi_{\text{sample}} \cong \frac{Qk}{(\varepsilon_r + 1)}\left(\frac{R^2 - Rh + h^2}{R^2 h}\right). \tag{21}$$

Equation (21) indicates that the potential difference depends on the trapped charge Q, working distance h, and radius of the charged disc R. The first question in this study is to determine the relation between the potential distribution and the properties of the electron mirror effects (EMEs). Using Eq. (21) together with the parameters $\varepsilon_r \approx 3.43$, $Q = 0.089$ pC at $h = 33$ mm, $Q = 0.3$ pC at $h = 20$ mm, $Q = 0.431$ pC at $h = 10$ mm, and R ranged from -0.3 to 0.3 mm, we note the potential distribution was close to a Gaussian distribution as shown in Figs. 4(a)–4(c). Since the potential depends on the working distance h, it can be increased by decreasing the working distance h. Figure 4(a') shows the EME, obtained at $h = 33$ mm working distance. It is clearly observed from Fig. 4(a') that the brightness at the upper right corner of the image is larger than that of the lower left corner (dark).

The brightness depends on the number of SEs which reach the ETD detector; therefore, the top wall of the FIB-SEM chamber which is close to the side of the ETD detector appears brighter than the opposite side of the top wall of the FIB-SEM chamber in EME, because of the large numbers of SEs which are emitted from the top wall of the FIB-SEM chamber and reach the detector from the nearest side.

Figures 4(b') and 4(c') show the mirror images obtained at different working distances $h = 20$ mm and $h = 10$ mm, respectively. It appears that the brightness of EME is inversely proportional to the working distance. The observed correlation between the brightness and the working distance might be explained in this way; a high value of potential which is created above the surface of the PET sample at $h = 10$ mm compared with the potential at $h = 20$ mm and $h = 33$ mm. Consequently, the greatest incident electrons can be accelerated toward the top of FIB-SEM system at $h = 10$ mm; therefore, a large number of reflected electrons interact with the top chamber of the FIB-SEM system to produce a large number of the SEs which are emitted from it to the ETD detector.

By comparing the EMEs from Figs. 4(a'), 4(b'), and 4(c'), it can be seen that the brightness in the upper right corner of images 4(b') and 4(c') is greater than that in image 4(a'); however, the resolution is lower. These differences in brightness and resolution can be explained as follows: reducing the working distance might lead to high values of the SE yield (high intensity) of the top of FIB-SEM system near the ETD detector, and the detector speed is obviously critical, where a large percentage of the SEs measured have the same energy, which contributes to reducing the number of detected electrons, consequently, reducing the resolution of the ETD detector.

3.2 *Estimate of Trapped Charge Q*

The second question in this research was the relationship between the trapped charge Q, h, and $\Delta\varphi$. From Eq. (21), the number of charges that are trapped on the surface of the insulator is given by

$$Q \cong \frac{\Delta\varphi R^2 h}{k(\varepsilon_r + 1)(R^2 - Rh + h^2)}. \tag{22}$$

As soon as the electron gun irradiates the sample, the sample charges negatively and a positive charge is induced on the disc by electrostatic influence. For a given working distance, $\Delta\varphi$, and R is only a function of Q.

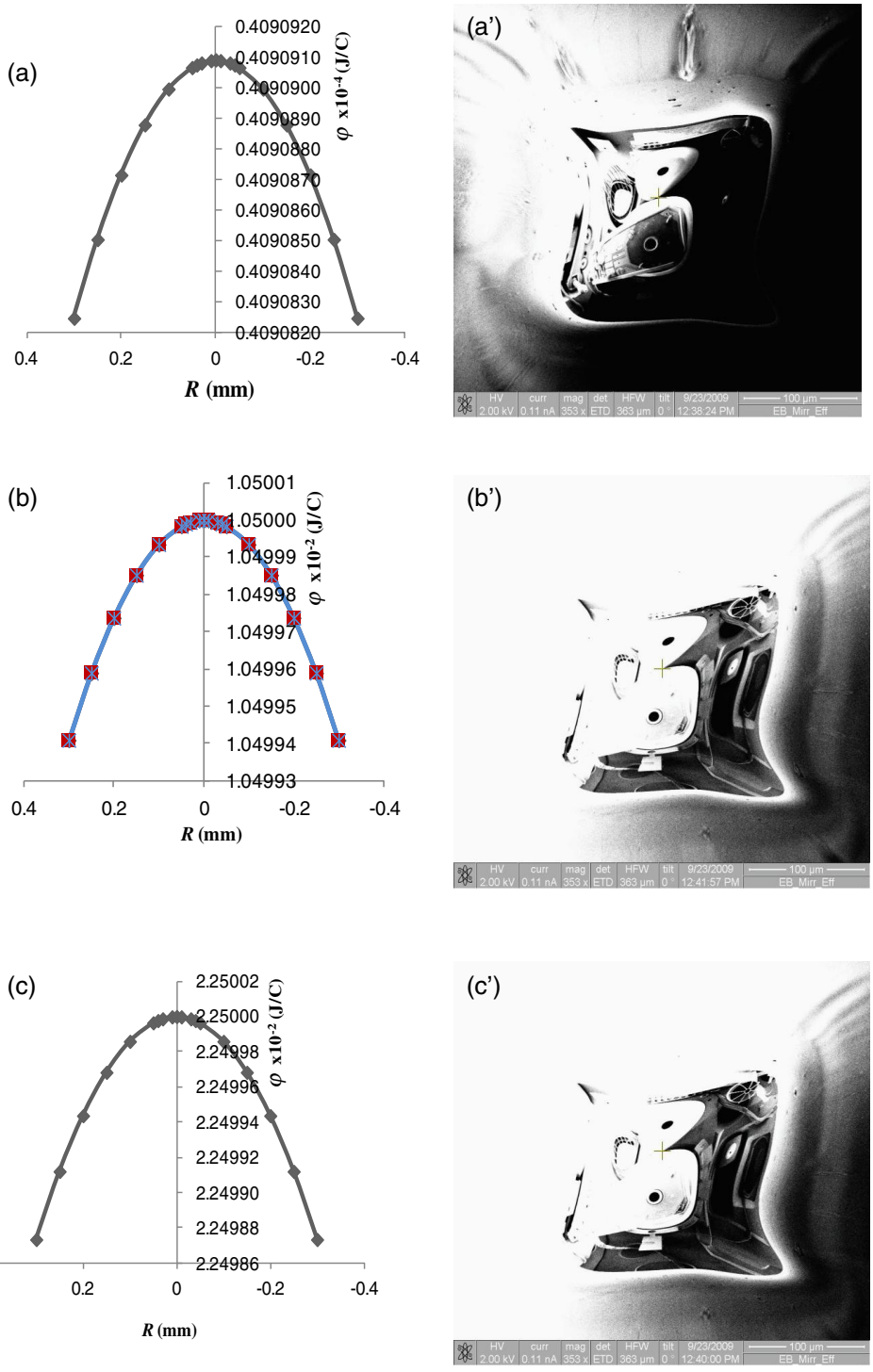

Fig. 4 The potential distribution of charged disc and the mirror images of a PET sample with $\Delta\varphi = 2$ kV, a current of 0.11 nA and magnifications 353× for different: (a) $h = 33$ mm (b) $h = 20$ mm (c) $h = 10$ mm.

Figure 5(a) shows the measured trapped charge Q versus the working distance with a constant radius of the charged disc R of 0.3 mm, an accelerating voltage $\Delta\varphi$ of 1 kV and the energy of the electron η of 500 eV. The negative trapped charge increases by reducing the working distance. Q varies with the working distance h according to Eq. (22).

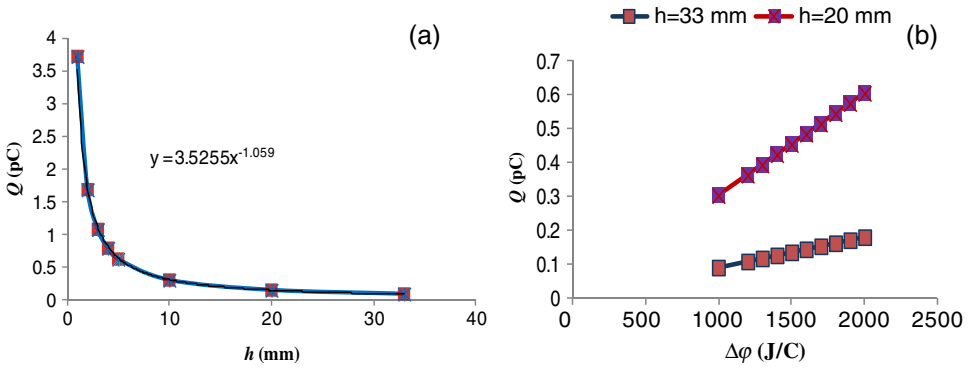

Fig. 5 The trapped charges Q as a function of (a) the working distance h (b) electric potential difference $\Delta\varphi$.

$$Q = \frac{3.5255}{h^{1.059}}. \tag{23}$$

The equation shows that a high charge concentration that builds up on the insulator surface is inversely proportional to the working distance h as shown in Eq. (23).

This result may be explained by the fact that the electric field increases by reducing the working distance h for a given value of the electrical potential difference $\Delta\varphi = 1$ kV, as shown in Eq. (24):

$$E = \frac{\varphi_{\text{gun}} - \varphi_{\text{sample}}}{h} = \frac{\Delta\varphi}{h}. \tag{24}$$

Equation (25) provides a shortcut to understanding the effect of the electric field E on the electrons' acceleration a_e, where an increasing in the electric field leads to an increase in the acceleration of the electrons a_e which strike the PET sample with high energy to produce a large amount of the trapped charge Q.

$$a_e = \frac{qE}{m}, \tag{25}$$

where m and q are the mass and charge of the electrons, respectively. Figure 5(b) shows the variation of the electric potential difference $\Delta\varphi$ with the trapped charges' concentration Q for two values of the working distance $h = 33$ and 20 mm.

Q varies linearly with $\Delta\varphi$. A possible explanation for this might be that the kinetic energy of the incident electron beam increases with an increase in the electric potential difference $\Delta\varphi$ at a constant working distance h as shown in Eq. (26).

$$\frac{1}{2}mv^2 = q\frac{\Delta\varphi}{h}, \tag{26}$$

where v is velocity of the electron. For an electric potential difference of $\Delta\varphi = 1$ kV, the trapped charges' concentration $Q = 0.089$ pC at $h = 33$ mm, and $Q = 0.3$ pC at $h = 20$ mm.

3.3 *Differential Cross Section $d\sigma/d\Omega$*

Differential cross sections $d\sigma/d\Omega$ provide valuable insights on relativistic interactions, which control the electron scattering dynamics and give the number of scattered particles in a certain solid angle $d\Omega$.

The general geometry of a scattering experiment is presented in Fig. 6. Incident electrons interact with the negative charged which accumulated on the surface of the PET sample, which reflects some of the electrons through an angle θ relative to the original beam direction. According to Rutherford scattering, the differential cross-section $d\sigma/d\Omega$ can be given by[21]

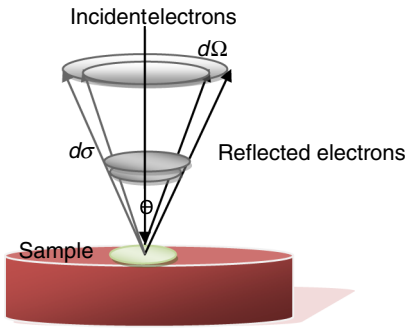

Fig. 6 Schematic of scattering incident electrons.

$$\frac{\mathrm{d}\sigma}{\mathrm{d}\Omega} = \left(\frac{kQe}{4\eta}\right)^2 \sin^{-4}\left(\frac{\theta}{2}\right), \tag{27}$$

where η is the energy of a primary electron.

Substituting Eq. (22) into Eq. (27), the differential cross-section $\mathrm{d}\sigma/\mathrm{d}\Omega$ can be obtained

$$\frac{\mathrm{d}\sigma}{\mathrm{d}\Omega} = \left[\frac{\Delta\varphi R^2 he}{4(\varepsilon_r + 1)(R^2 - Rh + h^2)\eta}\right]^2 \sin^{-4}\left(\frac{\theta}{2}\right). \tag{28}$$

3.3.1 *h, η, and θ dependence of dσ/dΩ*

In this section, we demonstrate the effect of the working distance h, scattering angle θ, and electric potential difference $\Delta\varphi$ on the differential cross-section $\mathrm{d}\sigma/\mathrm{d}\Omega$ of the reflected electrons. Based on the charging effect, electrons with energies of 500, 750, and 1000 eV are scattered off the PET sample. Given that the differential cross-section $\mathrm{d}\sigma/\mathrm{d}\Omega$ of this reaction is a function of the scattering angle θ for the following assumptions, the differential cross-section $\mathrm{d}\sigma/\mathrm{d}\Omega$ is inversely proportional to h and the scattering angle θ.

Our results, shown in Fig. 7(a), indicate the relation between $\mathrm{d}\sigma/\mathrm{d}\Omega$ and the working distance h for the energy of electrons of $\eta = 500$ eV and for different scattering angles $\theta = 20$ deg, 30 deg, and 50 deg.

Hence, for a given $h = 5$ mm, we estimate the differential cross-section as $\mathrm{d}\sigma/\mathrm{d}\Omega = 2.3 \times 10^{-9}$ m^2/sr at $\theta = 20$ deg, $\mathrm{d}\sigma/\mathrm{d}\Omega = 4.66 \times 10^{-10}$ m^2/sr at $\theta = 30$ deg, and $\mathrm{d}\sigma/\mathrm{d}\Omega = 6.56 \times 10^{-11}$ m^2/sr at $\theta = 50$ deg and for a given $\theta = 20$ deg $\mathrm{d}\sigma/\mathrm{d}\Omega = 1.32 \times 10^{-10}$ m^2/sr at $h = 20$ mm, and $\mathrm{d}\sigma/\mathrm{d}\Omega = 4.79 \times 10^{-11}$ m^2/sr at $h = 33$ mm.

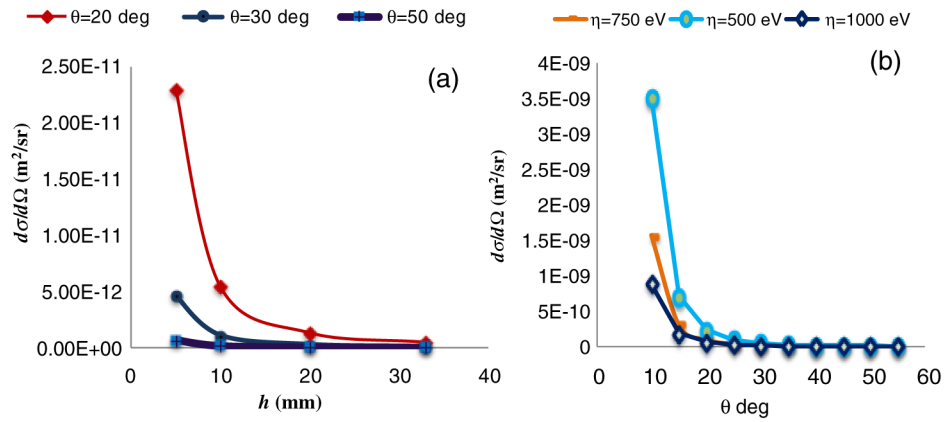

Fig. 7 The differential cross-section $\mathrm{d}\sigma/\mathrm{d}\Omega$ of scattering electron versus with (a) the working distance h (b) scattering angle θ.

The observed correlation between the differential cross-section and scattering angle θ might be explained in this way: when the scattering angle $\theta = 20$ deg, the potential above the surface of the PET sample is high, according to Sec. 3.1. In addition, a possible explanation for the correlation between the differential cross-section and the working distance h is that the difference potential increase with a decrease in the working distance h leads to a high electric field which reflected the incident electrons.

The results, shown in Fig. 7(b), demonstrated that the relation between the differential cross-section and scattering angle θ is inversely proportional for different electron energies $\eta = 500$, 750, and 1000 eV.

By fixing the working distance at $h = 33$ mm, and $\theta = 10$ deg, the differential cross-section as $d\sigma/d\Omega = 3.5 \times 10^{-9}$ m^2/sr at $\eta = 500$ eV, $d\sigma/d\Omega = 1.54 \times 10^{-9}$ m^2/sr at $\eta = 750$ eV, and $d\sigma/d\Omega = 0.98 \times 10^{-9}$ m^2/sr at $\eta = 1000$ eV. For incident electrons with low-energy, the differential cross-section is high because the surface potential that arises from the trapping of negative charges reflects the electrons with high acceleration.

3.3.2 $\Delta\varphi$ dependence of $d\sigma/d\Omega$

Using Eq. (28) and the parameters $h = 33$ mm, $R = 0.3$ mm, and $\eta = 500$ eV, we find a relation between $d\sigma/d\Omega$ and $\Delta\varphi$. Fig. 8(a) compares the differential cross-sectional $d\sigma/d\Omega$ as a function of the difference potential $\Delta\varphi$ at different scattering angles $\theta = 20$ deg, 30 deg, and 50 deg.

This figure clearly shows that the differential cross-section $d\sigma/d\Omega$ is directly proportional to the difference potential $\Delta\varphi$. A possible explanation for these results may be that the accumulation of static charges can be increased by increasing the difference potential $\Delta\varphi$ and more charges appear on the surface of the sample (PET), therefore, the magnitude of the electric field at that surface also increases. Finally, the strength of the field becomes great enough to repel more incident electrons, increasing the number of scattered electrons.

At a given $\Delta\varphi$, the differential cross-section $d\sigma/d\Omega$ is inversely proportional to the scattering angle θ. This result may be explained by the fact that the charge distribution is approximately Gaussian on the charged disc. However, a high density of charges at the center of the disc scatters a large number of incident electrons in a direction closer to the incident electrons (small angle) according to the Coulomb force.

The differential cross-sectional $d\sigma/d\Omega$ can be calculated by using the parameters $R = 0.3$ mm, $h = 33$ mm, $\theta = 30$ deg and Eq. (28) at $\eta = 500$, 750, and 1000 eV, Fig. 8(b), illustrates that the differential cross-sectional $d\sigma/d\Omega$ increases when decreasing the electron energy η. This result may be explained by the fact that the interaction points of incident electrons with electrostatic potential above the surface sample (PET) are different depending on the energies of the incident electrons, where the interaction path of the electrons that have $\eta = 500$ eV is

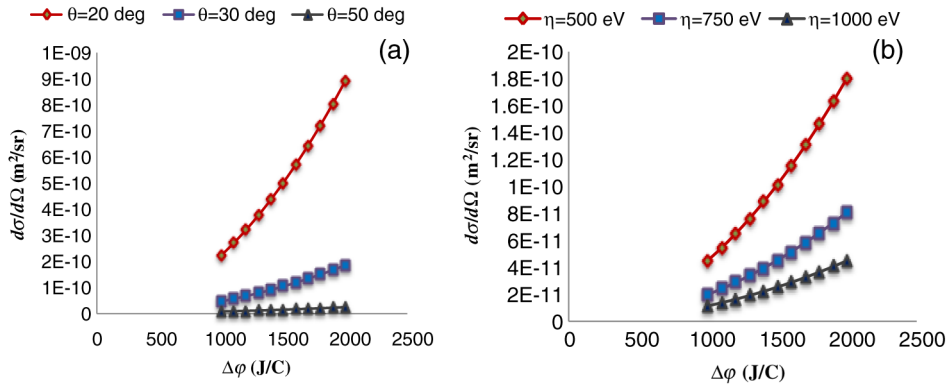

Fig. 8 The differential cross-section $d\sigma/d\Omega$ of scattering electrons as a function of the potential difference (a) $\eta = 500$ eV, $h = 33$ mm, $R = 0.3$ mm, and $\Delta\varphi = 1$ kV for different $\theta = 20$ deg, 30 deg, and 50 deg (b) $h = 33$ mm, $R = 0.3$ mm, $\theta = 30$ deg, and $\Delta\varphi = 1$ kV for different $\eta = 500$, 750, and 1000 eV.

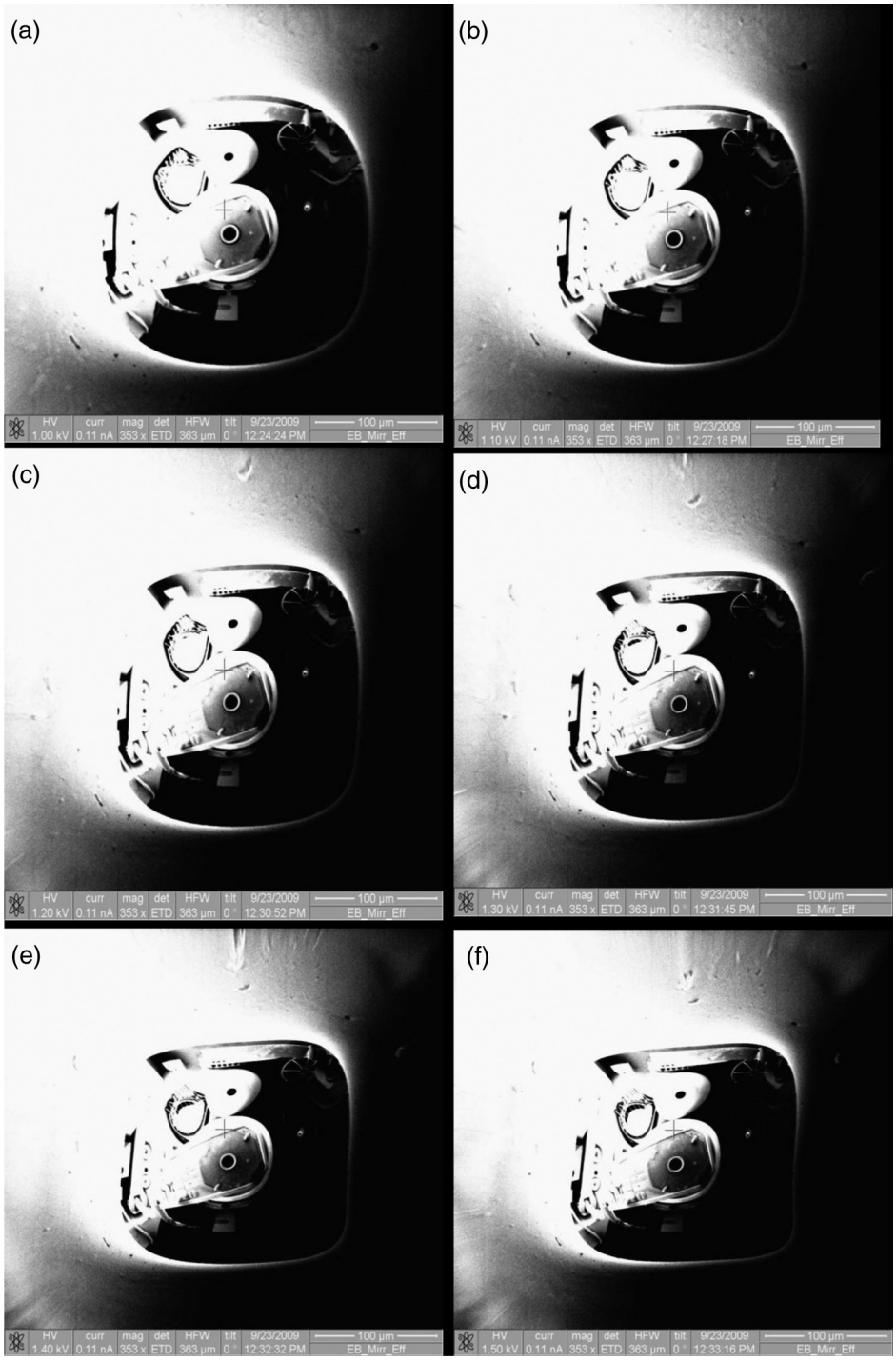

Fig. 9 Electron mirror images at different potential differences $\Delta\varphi$ (a) =1 kV, (b) =1.1 kV, (c) =1.2 kV, (d) =1.3 kV, (e) =1.4 kV, (f) =1.5 kV, (g) =1.6 kV, (h) =1.7 kV, (i) =1.8 kV, (j) =1.9 kV, and (k) =2 kV.

less than those which have $\eta = 750$ and 1000 eV. Furthermore, the electrostatic potential above the sample provides a high level of work on the incident electrons of 500 eV. Consequently, the landing energy of the incident electrons is reduced and the electric field may be strong enough to reflect it from the area close to the electron gun. Therefore, the differential cross-sectional $d\sigma/d\Omega$ that has $\eta = 500$ eV is higher than those which have $\eta = 750$ and 1000 eV.

Figure 9 shows the mirror images of the sample (PET). This can provide information about the properties of EMEs, in the case of a changing $\Delta\varphi$ and fixation of the current to 0.11 nA, with

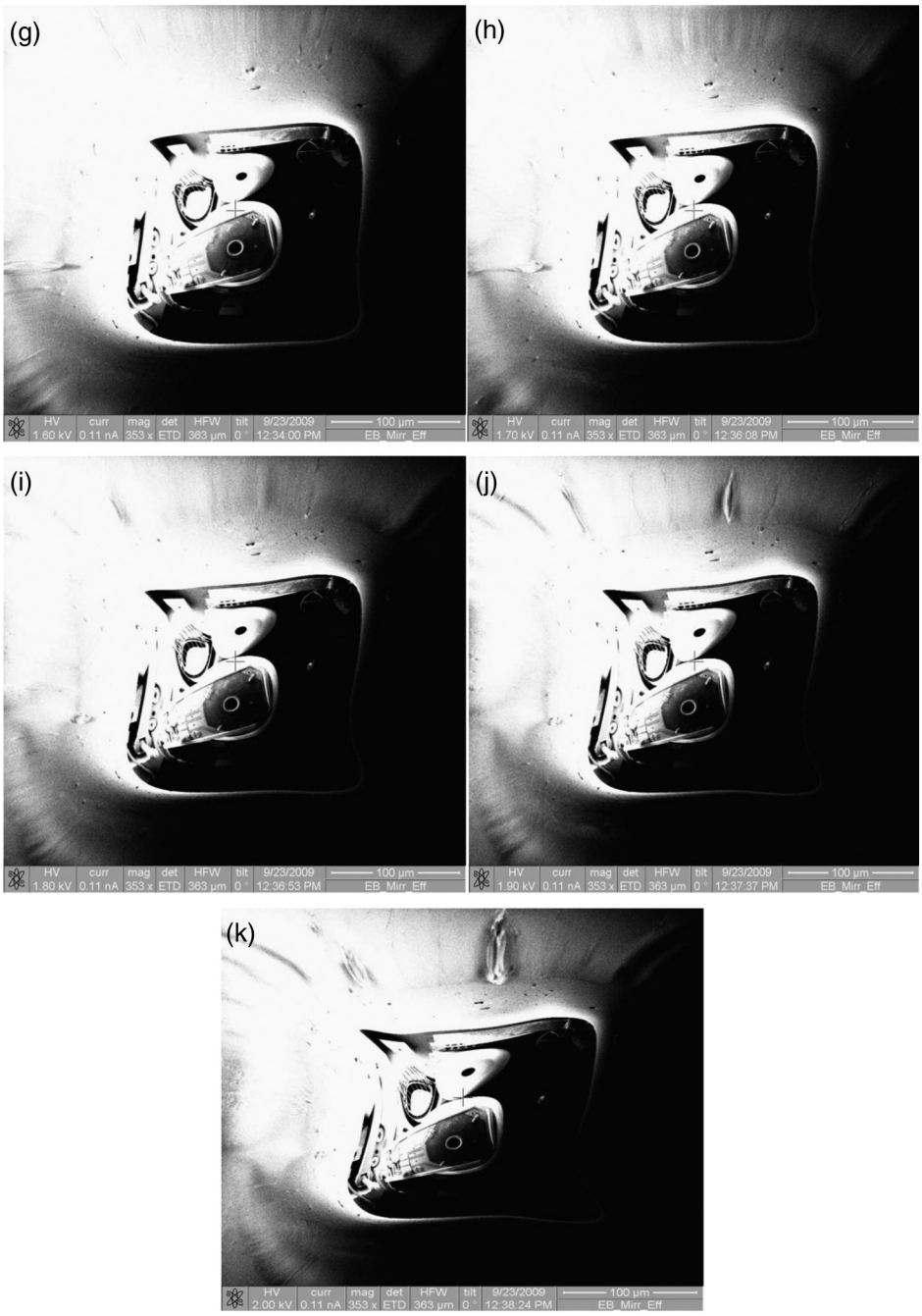

Fig. 9 *(Continued)*

magnifications of 353×, and a working distance of 33 mm of the FIB-SEM system. The most interesting finding was that an increase of the potential difference $\Delta\varphi$ gives rise to a brightness and resolution increases: the images with a high potential difference will have more details than those with a low potential difference. A possible explanation for this might be that the differential cross-section $d\sigma/d\Omega$ is high with increasing $\Delta\varphi$. Another important finding was that the shape of EMEs appears distorted when increasing the potential difference $\Delta\varphi$ from 1 to 2 keV. The circular shape of the mirror images in Figs. 9(a) and 9(b) is converted to nearly rectangular shapes at images 9(c) and 9(d), with the shapes of the mirror images 9(e)–9(k) suffering deformation in the corners of the shapes. This result may be explained by the fact that the relationship between the incident electrons and the reflected electrons depends on the distribution of the trapped electrons in the specimen. When the potential difference $\Delta\varphi$ is increasing, this leads to the accumulation

irregular trapped electrons on the surface of the sample (PET). The irregularity of trapped electrons leads to building an irregular electric field in the space between the surface of the sample (PET) and the grounded chamber wall in the vacuum. This is an irregular electric field that tends to deform and bend the trajectories (paths) of reflected electrons and SEs.

4 Conclusions

The FIB-SEM system allows high-resolution, high-magnification imaging of conductive samples. The system fails for an insulator sample (PET) and the EME appears instead of an image of the sample.

The connectivity between the mathematical analysis and experiments can play a relevant role in the understanding of the basic features of the electrodynamics of the charging process of the (PET) sample and the properties of electron mirror images.

We derive a potential difference equation and include the parameter of FIB-SEM system such as the working distance h and parameters of the sample such as the radius of the charged disc R, the permittivity of the (PET) sample ε_r, and trapped charge Q. We use this equation to find the differential cross-section $\mathrm{d}\sigma/\mathrm{d}\Omega$ equation. The differential cross-section $\mathrm{d}\sigma/\mathrm{d}\Omega$ is one of the most important physical observations in scattering experiments. It can be motivated as follows: a detector usually records the number of particles scattered from the target into a certain solid angle.

The following conclusions can be drawn from the present study:

1. The trapped charge Q on the surface of a PET sample decreases with increasing h.
2. The distribution of the electric potential on the PET sample affects the acceleration of the reflected incident electrons.
3. The properties of the electron mirror images depend on the paths of SEs and the distribution of electric potential on the surface of the PET sample.
4. The differential cross-section $\mathrm{d}\sigma/\mathrm{d}\Omega$ of the reflected electrons is inversely related to the scattering angle θ and the working distance h.
5. $\mathrm{d}\sigma/\mathrm{d}\Omega$ is directly proportional to the difference potential $\Delta\varphi$ and the energy of the primary electrons η.

Acknowledgments

The authors would like to thank Prof. M. Milani, F. Croccolo, Prof. Daniela Candia, all staff of summer school 2009 and Department of Material Science at the Universit à degli Studi di Milano—Bicocca.

References

1. F. Croccolo and C. Riccardi, "Observation of the ion-mirror effect during microscopy of insulating materials," *J. Microsc.* **229**(1), 39–43 (2008).
2. H. Gong et al., "Charge trapping on different cuts of a single-crystalline a-SiO_2," *J. Appl. Phys.* **74**(3), 1944–1948 (1993).
3. M. Milani et al., "Rear window: looking at charged particles hitting a charged target in a FIB/SEM," *Microscopy: Science, Technology, Applications and Education*, A. Méndez-Vilas and J. Díaz, Eds., pp. 1741–1754, Formatex Research Center, Badajoz, Spain (2010).
4. J. Cazaux, "Some considerations on the secondary electron emission from electron-irradiated insulators," *J. Appl. Phys.* **85**(2), 1137–1147 (1999).
5. M. Dapor, M. Ciappa, and W. Fichtner, "Monte Carlo modeling in the low-energy domain of the secondary electron emission of polymethylmethacrylate for critical-dimension scanning electron microscope," *J. Micro/Nanolith., MEMS, MOEMS* **9**(2), 023001 (2010).
6. O. Jbara et al., "Charge implantation measurement on electron-irradiated insulating materials by means of a SEM technique," *Microsc. Microanal.* **10**(6), 697–710, (2004).
7. W. Zhou and Z. L. Wang, *Scanning Microscopy for Nanotechnology*, Springer, New York (2006).

8. C. R. Brundle, C. A. Evans, Jr., and S. Wilson, Eds., *Encyclopedia of Materials Characterization*, Butterworth-Heinemann, Stoneham, Massachusetts (1992).
9. L. Reimer, *Scanning Electron Microscope. Physics of Image Formation and Microanalysis*, pp. 119–121, Springer-Verlag, New York (1985).
10. T. Temga et al., "Conduction and t-rapping of electric charges in an anisotropic material after irradiation with an electron of trapping of beam: application to TiO_2 single crystal," *Nucl. Instrum. Method Phys. B* **245**(2), 519–527 (2006).
11. M. Belhaj et al., "An anomalous contrast in scanning electron microscope of insulators. The pseudo mirror effect," *Scanning* **22**(6), 352–356 (2000).
12. M. Belhaj et al., "Time dependent measurement of the trapped charge in electron irradiated insulators: application to Al_2O_3 sapphire," *J. Appl. Phys.* **88**(5), 2289–2294 (2000).
13. B. Vallayer et al., "Space charge measurement in a dielectric material after irradiation with a 30 kV electron beam: application to single-crystals oxide trapping properties," *Rev. Sci. Instrum.* **70**(7), 3102–3112 (1999).
14. H. J. Wintle, "Analysis of the scanning electron microscope mirror method for studying space charge in insulators," *J. Appl. Phys.* **86**(11), 5961–5967 (1999).
15. J. Liebault et al., "Advanced measurement techniques of spacecharge induced by an electron beam irradiation in thin dielectric layers," *J. Non-Cryst. Solids* **322**, 213218 (2003).
16. M. Milani, D. Bigoni, and C. Savoia, "Electron mirroring: control of electron transport and understanding of physical processes from SEM images," in *Proc. of ITP2009, Interdisciplinary Transport Phenomena VI: Fluid, Thermal, Biological, Materials and Space Sciences October 4-9*, Volterra, Italy, pp. 1–11 (2009).
17. Y. M. A. Al-zahy et al., "Characterizations of the mirror effects induced from a PET sample in SEM and FIB," in *Electron and Ion Microscopy and Micromanipulation: Common Principles and Advanced Methods in Applied Sciences*, M. D. Candia Carnevali and M. Milani, Eds., Proc. of Summer School, Società Editrice Esculapio ,Bologna, Italy (2009).
18. M. L. Hattali, N. Mesrati, and D. Tréheux, "Electric charge trapping, residual stresses and properties of ceramics after metal/ceramics bonding," *J. Eur. Ceram. Soc.* **32**(4), 717–725 (2012).
19. S. Babin, S. Borisov, and A. Ivanchikov, "Modeling of charge and discharge in scanning electron microscope," *Proc. SPIE* **7378**, 737818 (2009).
20. C. G. Someda, *Electromagnetic Waves*, 2nd ed., CRC Taylor & Francis, Boca Raton, Florida (2006).
21. N. J. Thomas, "Measuring beam intensities and cross sections using Rutherford scattering techniques," MSc Thesis, Department of Physics, University of Surrey, United Kingdom (2005).

Younis Mohamed Atiah Al-zahy has been an associate professor of physics in the Department of Science at Misan University since 2006. He received his PhD and MSc degrees in the College of Physical Science from Al-Mustansiriya University, Iraq, in 2006 and 1998, respectively. Currently, he works at the Laboratory of Laser Technology, and the College of Science as a lecturer in physics. He has published many papers in the fields of fiber lasers and scanning electron microscope of insulators.